Benemérita Universidad Autónoma de Puebla

Facultad de Ciencias Físico Matemáticas

Study of initial state fluctuations in pp and pPb as non-equilibrium systems

Tesis presentada al

Posgrado en Física Aplicada

como requisito parcial para la obtención del grado de

Maestro en Ciencias

por

Fernando Enrique Neri Huerta

Asesores:

Dra. Iraís Bautista Guzmán

Dr. Humberto Antonio Salazar Ibargüen

Puebla, Pue.
Julio de 2023

Benemérita Universiddad Autónoma de Puebla

Facultad de Ciencias Físico Matemáticas

Study of initial state fluctuations in pp and pPb as non-equilibrium systems

Tesis presentada al

Posgrado en Física Aplicada

como requisito parcial para la obtención del grado de

Maestro en Ciencias

por

Fernando Enrique Neri Huerta

Asesores:

Dra. Iraís Bautista Guzmán

Dr. Humberto Antonio Salazar Ibargüen

Puebla, Pue.
Julio de 2023

Título: Study of initial state fluctuations in pp and pPb as non-equilibrium systems
Estudiante: Fernando Enrique Neri Huerta

Comité

Presidente:

Dr. Justiniano Lorenzo Díaz Cruz
FCFM-BUAP

Secretario:

Dra. María Isabel Pedraza Morales
FCFM-BUAP

Vocal:

Dr. Marco Antonio Arroyo Ureña
FCFM-BUAP

Suplente:

Dr. Enrique Varela Carlos
FCFM-BUAP

Asesores:

Dra. Iraís Bautista Guzmán
FCFM-BUAP

Dr. Humberto Antonio Salazar Ibargüen
FCFM-BUAP

Contents

A mi mamá y mi papá: la persona con el corazón más grande que he conocido y quién respondió mis primeras preguntas.

A los amigos con los que coincidí en este proceso, les debo muchísimo.

Mi sincera gratitud a la Dra. Iraís por su infinito apoyo y al Dr. Humberto que me apoyaron enormemente a lo largo del trayecto.

En el transcurso del posgrado pude apreciar de mejor manera a los profesores que me apoyaron y me guiaron al camino que elegí: Mtra. Laura Xochicale, Mtra. Rebeca Zambrano, Dr. Jorge Velazquez, Dra. Isabel Pedraza, Dr. Héctor Novales.

Finalmente, a la sociedad mexicana que mediante el CONACyT y la BUAP, me otorgó una beca y las instalaciones brindadas para realizar un posgrado, respectivamente.

Uno debe orientarse por aquello que más le sirva para ayudar al bien de la sociedad: K. Marx.

Resumen

En este proyecto se propone un estudio de las fluctuaciones del estado inicial en colisiones de pp (protón-protón), pPb (protón-plomo) y $PbPb$ (plomo-plomo) a las energías del Gran Colisionador de Hadrones (LHC), como una forma de analizar el estado que se forma en los eventos de alta multiplicidad de dichos sistemas y la relación con el Plasma de Quarks y Gluones (QGP).
En particular, estudiar el efecto de las fluctuaciones que se asocian al estado inicial como lo son la fluctuaciones en el espectro de multiplicidad. Esto permite analizar la temperatura y densidad de energía, así como la caracterización posible por especie, de manera local y global para cada evento de la colisión.
El análisis se presenta bajo el Modelo de Percolación de Cuerdas de Color (CSPM), como una propuesta para las fluctuaciones de momento transverso y es comparado con la distribución mecánico estadística Tsallis; dado la exitosa representación con la cual recrean los espectros de momento trasverso para hadrones en colisiones de iones pesados y pp [1].

Abstract

This project proposes a study of the fluctuations of the initial state in collisions of pp (proton-proton), pPb (proton-lead) and $PbPb$ (lead-lead) at the energies of the Large Hadron Collider. (LHC) as a way of analyzing the state that is formed in the high multiplicity events of these systems and the relationship with the Quarks and Gluon Plasma (QGP).
In particular, to study the effect of fluctuations that are associated with the initial state, such as fluctuations in the multiplicity spectrum. This allows analyzing the temperature and energy density, as well as the possible characterisation by species, locally and globally for each collision event.
The analysis is presented under the Color String Percolation Model (CSPM), as a proposal for transverse momentum fluctuations and is compared with the Tsallis distribution, given the successful representation with which they recreate the transverse momentum spectra for hadrons in pp collisions and heavy ions [1].

Introduction

The ordinary matter that surrounds us and with which we interact daily is made up of atoms that in turn are made up of electrons that surround the nucleus that consists of protons and neutrons, and that keep confined (in the physical conditions in which we live) its constituents: quarks and gluons.
Quantum Chromodynamics (QCD) is the theory of strong interaction, that involves the color charge that quarks and gluons have. The quarks and gluons are not asymptotically free states as occurs in electrodynamic theory. The theory shows that they are confined states in composite structures called hadrons, this process is known as confinement, which is an open problem.
In the 1970s, it was analyzed that under conditions of high temperature and/or nuclear density a process of deconfinement of quarks and gluons could be reached, forming a compound called Quark-Gluon Plasma (QGP) [2, 3].
It is postulated that this state occurred a few microseconds after the *Big Bang*, when it was in a small space and as the Universe expanded it began to cool down and the process of confinement and formation of hadrons began, as are protons and neutrons.
The latest experimental efforts in accelerator and detector physics have contributed to study the state formed in collisions of high nuclear density; as are the experiments: ALICE, CMS, and ATLAS at the LHC, as well as STAR and PHENIX at RHIC (Relativistic Heavy Ion Collider) at Brookhaven National Laboratory (BNL). It was recently observed that even pp and pPb collisions produce events with a high production of particles, with characteristics similar to those found in nuclear collisions.
The study of temperature fluctuations gives us information about the thermalization of the system and the existence or not of a phase transition; in addition to the fact that the temperature fluctuations in the collisions pp maintain information about the fluctuations present in the initial state and help us to understand and describe the existence of phase transitions in matter where they occur in the created systems.
Particle collision experiments attempt to understand the thermodynamic properties of strongly interacting systems. Due to the nature of the collision, the state immediately after the collision constitutes a system imbalance. It is known that fluctuations in the initial conditions lead to specific structures in the final hadronic spectra.
This work proposes to carry out the study of temperature fluctuation indirectly on high multiplicity events in small systems, under the String Percolation Theory and its comparison with the statistical mechanical approach of the Tsallis distribution and to study their behavior with respect to said observables in nuclear collisions, this in order to characterize these systems and explain their differences with the collective state formed in nuclear collisions.

Chapter 1

Particle Physics

Field and particle physics is the branch of physics that studies the fundamental components and interactions of matter. Currently, four fundamental interactions or forces are known in the universe: strong, weak, electromagnetic, and gravitational; distinguished by their scope and different magnitudes. [4].
The gravitational interaction is the weakest in magnitude, but has infinite range; the electromagnetic one also has infinite range, but stronger than the gravitational force. The weak interaction, like the strong force, has small ranges, on a subatomic scale, but of magnitude less than the electromagnetic one. Being the strong interaction, the largest in magnitude.

Interaction	Theory	Mediators	Relative Strength	Range of Interaction (m)
Strong	QCD	gluon	10^{38}	10^{-15}
Electromagnetic	QED	photon	10^{36}	∞
Weak	Electroweak	W±, Z	10^{25}	10^{-18}
Gravitational	General Relativity	graviton (Theorized)	1	∞

Table 1.1: The four fundamental interactions, their relative strengths, and their mediators [5].

Each of the interactions has been studied giving rise to a theory that describes it. From the study of gravity by Sir Isaac Newton, as the law of Universal Gravitation. As well as its subsequent generalization by Albert Einstein in the theory of General Gravitation.
The theory that describes the electromagnetic force is Electrodynamics, it precedes the classical formulation of James Clerk Maxwell. The quantum theory of electrodynamics was perfected by Shin'ichirō Tomonaga, Richard Feynman, and Julian Schwinger in the 1940s [4].
The weak interaction, which explains nuclear beta decay, was a phenomenon unknown to classical physics; its theoretical description was of a relativistic quantum type from the beginning. The first advances were proposed by Enrico Fermi in 1933; it was supplemented by Tsung-Dao Lee, Chen Ning Yang, Feynman, Murray Gell-Mann and others in the 1950s. Obtaining its current explanation by Glashow, Weinberg and Salam in the 1960s. The strong interaction stems from the first efforts proposed by Hideki Yukawa in 1934 [6], until the emergence of Quantum Chromodynamics in the 1970s.

1.1 Standard Model

The Standard Model (SM) is a quantum field theory that incorporates three of the known fundamental interactions of matter, (strong, weak and electromagnetic), through the exchange of the corresponding vector fields of spin 1 [7].
It is a gauge theory based on local symmetries of the group $SU(3)_C \times SU(2)_L \times U(1)_Y$, where the subscripts denote *color, left-handed chirality* and *weak hypercharge*, respectively. The gauge group determines the interactions and the number of their mediators, associated with the group generators, with which we have:

- 8 massless bosons (gluons) corresponding to the 8 generators of $SU(3)_C$, mediate the strong force interaction.
- 3 massive gauge bosons ($W^{\pm}$, Z), associated with the generators of $SU(2)_L$
- 1 massless gauge boson (γ), associated with $U(1)_Y$.

In the Standard Model, the interactions of the weak force and electromagnetism are unified in the electroweak theory [8–10], of the symmetry group $SU(2)_L \times U(1)_Y$. Since there is no mixing with the sector $SU(3)_C$ and its symmetry is not broken, the study of the electrodeweak theory can be independent of the theory of strong interactions (Quantum Chromodynamics).
Initially it is constituted with gauge bosons and non-massive fermions, historically the need for massive particles was a problem of the SM.
Subsequently, through a mechanism discovered in 1964, the mass terms are theoretically generated by the spontaneous breaking of the local gauge symmetry; a mechanism discovered by P.W. Higgs, F. Englert, R. Brout, G.S. Guralnik, C.R. Hagen, and T.W.B. Kibble, named *Higgs Mechanism* [11–15]. In addition, G. 't Hooft and M. Veltman [16] provided the renormalization of the model, thereby adding feasibility to the theory.
One of the most important discoveries in particle physics was the observation of the boson associated with this mechanism, the *Higgs boson*. It was reported in 2012 at CERN, by the ATLAS and CMS collaborations [17, 18].

1.1.1 Fermions

All the matter that surrounds us is made up of elementary particles, they are classified into two types, according to the statistics they obey: fermions or bosons [19].
Fermions are half-integer spin particles, which obey the Fermi-Dirac statistics, the fermionic matter content consists of three families of quarks and three families of leptons, differing only by the value of mass. These families are described in Table 1.2.

Fermions	1^{st} Generation	2^{nd} Generation	3^{rd} Generation
Quarks:	u (up),	c (charm),	t (top),
	d (down),	s (strange),	b (bottom),
Leptons:	ν_e (electron neutrino),	ν_μ (muon neutrino),	ν_τ (tau neutrino)
	e (electron),	μ (muon),	τ (tau).

Table 1.2: Quark and lepton families [7].

Quarks are distinguished by participating in all interactions, electromagnetic, weak, strong, and gravitational; and leptons, having no color charge, do not interact with the strong force.
The lightest and most stable particles make up the first generation, the heaviest and most unstable make up the second and third. The stable matter of the universe is composed of particles that belong to the first generation [20].

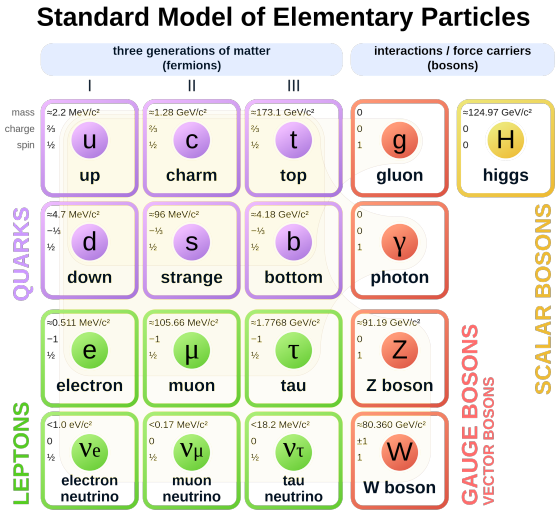

Figure 1.1: Elementary particles of the Standard Model [21]

1.1.2 Bosons

Bosons are particles with integer spin, which obey the Bose-Einstain statistic. They are the mediating particles of the interactions according to the exchange in the corresponding interaction, in addition to quantizing the respective field, they are divided into gauge bosons (vectorial) and scalar bosons (Higgs boson) [12]. Their characteristics are described in Table 1.3.

Boson	Mass (GeV)	Lifetime (s)	Charge (e)
γ (photon)	$< 2 \times 10^{-25}$	∞	0
$W\pm$	80.396 ± 0.061	$(3.195 \pm 0.077) \times 10^{-25}$	± 1
Z	91.187 ± 0.007	$(2.643 \pm 0.007) \times 10^{-25}$	0
g(8 gluons)	0	∞	0
Higgs	125.25 ± 0.1	2.1×10^{-22}	0

Table 1.3: Bosons in the Standard Model. [7, 22].

1.2 Quantum Chromodynamics

Hadrons, like protons and neutrons are responsible for more than 99% of the mass of all visible matter in our universe and are made up of quarks [23]. The strong interaction unites quarks and gluons within hadrons, it also determines the union between hadrons; a particular case is the formation of atomic nuclei. However, like the weak interaction, it only acts at subatomic distances, being limited to energies and temperatures below 1 MeV or 10^8 K [24]. Strong integration between fundamental particles has been satisfactorily described by a non-Abelian gauge theory, called Quantum Chromodynamics.

The path from nuclear physics to QCD divided into the era of nuclear spectroscopy can be seen; ending with the quark model. And followed by the deep inelastic scattering experiments, giving way

to the quark parton model. Finishing with the measurements of the interaction between quarks. In the late 1960s, studies of classification, mass spectra, and hadronic interaction suggested a composition by more fundamental elements, quarks.
Also, in the 1950s and 1960s, there was a general idea that strong interactions could not be described in the perturbative sense of quantum field theory methods.
The development of high energy physics in the second half of the 20th century was linked to the construction of large accelerators. The discovery of the existence of three baryons, Δ^{++}, Δ^{-}, Ω^{-}, formed by three quarks *uuu*, *ddd* and *sss* respectively, violated the Pauli Exclusion Principle. Color was introduced by O. Greenberg as a new quantum number to restore the Pauli principle: since quarks are particles with spin 1/2 [25], two quarks of the same type could not have the same quantum numbers. The interaction between the quarks is done through the exchange of gluons, which are the color carriers. However, in 1973 the property of asymptotic freedom of non-Abelian field theories was discovered. Asymptotic freedom allows a non-perturbative treatment of the strong interaction on small scales.
Events like the above, led to the formulation of a quantum field theory for strong interactions.

Quantum Chromodynamics (QCD) is the quantum theory of strong interaction based on the symmetry group $SU(3)_C$, where C, denotes a new degree of freedom called *color*. It dates back to 1964, when Murray Gell-Mann [26], and independently George Zweig [27], postulated the existence of quarks. It is a theory based on the concepts of color charged quarks, interaction between color quarks resulting from the exchange of gluon fields and local gauge symmetry.

1. Quarks: They are fundamental components of matter with half-integer spin, with the properties shown in the table 1.4.
   They have similar properties such as fractional electric charge, color charge and are only distinguished by the mass[1].

Generation	Quark	Charge(Q/e)	Mass(MeV)
I	up	2 / 3	$2.16^{+0.49}_{-0.26}$
	down	-1 / 3	$4.67^{+0.48}_{-0.17}$
II	charm	2 / 3	$1.27 \pm 0.02 \times 10^3$
	strange	-1 / 3	$93.4^{+8.6}_{-3.4}$
III	top	2 / 3	$172.69 \pm 0.30 \times 10^3$
	bottom	-1 / 3	$4.2^{+0.03}_{-0.02} \times 10^3$

Table 1.4: Quarks in the Standard Model [22]

.

   Experimentally, the non-observation of quarks in isolation is expressed in theory by postulating the *color confinement*. The quarks are physically grouped as *neutral color* particles, that is to say that the constituents add up the three color charges (hadrons: protons, neutrons, etc.), or they cancel out in pairs (quark-antiquark), a color and its anticolor (mesons: pion, kaon, etc.).

2. Gluons: They are the mediators of the strong force, they are non-massive vector bosons, with

[1]Since quarks are not freely observed, there are two types of mass for them, *current* and *constituent*. The mass of a quark is a parameter of the Lagrangian of QCD that describes the interaction of quarks. These masses are called *current mass* of quarks and it depends on the momentum scale and the renormalization scheme. In the *constituent* quark model, hadrons are united states of quasi-particles, which are valence quarks, surrounded by gluons and quark-antiquark pairs. However, the masses are phenomenological parameters that must be fitted to the mass spectra of experimental hadrons. The masses of the table 1.4, are of the type *current* of the quark u, d, s are estimated in the $\overline{\text{MS}}$ scheme, at a scale of $\mu \approx 2$ GeV. The mass of the *top* quark is measured directly.

two polarizations, which interact with themselves and with quarks, in addition to 8 different types of gluons.

3. Local gauge symmetry: It implies the invariance of the Lagrangian under a continuous set of local transformations. The corresponding gauge group in QCD is SU(3).

Each quark field $q(x)$, $(q = u, d, c, s, t, b)$ is assumed to have three color degrees of freedom:

$$q(x) = \begin{pmatrix} q_1(x) \\ q_2(x) \\ q_3(x) \end{pmatrix}. \tag{1.1}$$

The transformation of the quark fields under $\mathrm{SU(3)_C}$, is given under local transformations given by:

$$q(x) \to q'(x) = U(\underline{\theta}(x))q(x). \tag{1.2}$$

With:

$$U(\underline{\theta}(x)) = \exp\left(i\sum_{a=1}^{8}\theta_a(x)L_a\right). \tag{1.3}$$

Where $L_a = \lambda_a/2$, are the generators of $\mathrm{SU(3)_C}$; λ_a. The generators are matrices 3×3 of null trace, hermitian. Often written on a standard basis $T^a = \frac{1}{2}\lambda^a$, with λ^a being the Gell-Mann-Matrices:

$$\lambda^1 = \begin{pmatrix} 0 & 1 & 0 \\ 1 & 0 & 0 \\ 0 & 0 & 0 \end{pmatrix}, \quad \lambda^2 = \begin{pmatrix} 0 & -i & 0 \\ i & 0 & 0 \\ 0 & 0 & 0 \end{pmatrix}, \quad \lambda^3 = \begin{pmatrix} 1 & 0 & 0 \\ 0 & -1 & 0 \\ 0 & 0 & 0 \end{pmatrix},$$

$$\lambda^4 = \begin{pmatrix} 0 & 0 & 1 \\ 0 & 0 & 0 \\ 1 & 0 & 0 \end{pmatrix}, \quad \lambda^5 = \begin{pmatrix} 0 & 0 & -i \\ 0 & 0 & 0 \\ i & 0 & 0 \end{pmatrix}, \quad \lambda^6 = \begin{pmatrix} 0 & 0 & 0 \\ 0 & 0 & 1 \\ 0 & 1 & 0 \end{pmatrix},$$

$$\lambda^7 = \begin{pmatrix} 0 & 0 & 0 \\ 0 & 0 & -i \\ 0 & i & 0 \end{pmatrix}, \quad \lambda^8 = \frac{1}{\sqrt{3}}\begin{pmatrix} 1 & 0 & 0 \\ 0 & 1 & 0 \\ 0 & 0 & -2 \end{pmatrix}.$$

With the group structure constants f_{abc}:

$$f_{abc} = -\frac{i}{4}\,\mathrm{Tr}\left(\left[\lambda_a, \lambda_b\right]\lambda_c\right). \tag{1.4}$$

The Lagrangian of QCD is given by

$$\mathcal{L} = \sum_q \bar{\psi}_{q,a}\left(i\gamma^\mu\partial_\mu\delta_{ab} - g_s\gamma^\mu T^C_{ab}\mathcal{A}^C_\mu - m_q\delta_{ab}\right)\psi_{q,b} - \frac{1}{4}F^A_{\mu\nu}F^{A\mu\nu}, \tag{1.5}$$

where repeated indices are summed over. The γ^μ are the Dirac γ-matrices. The $\psi_{q,a}$ are quark-field spinors for a quark of flavor q and mass m_q, with a color-index a that runs from $a = 1$ to $N_c = 3$, i.e. quarks come in three "colors." Quarks are said to be in the fundamental representation of the SU(3) color group.

The $\mathcal{A}^C_\mu$ correspond to the gluon fields, with C running from 1 to $N_c^2 - 1 = 8$, i.e. there are eight kinds of gluon. Gluons transform under the adjoint representation of the SU(3) color group. The Gell-Mann-Matrices (T^C), encode the fact that a gluon's interaction with a quark rotates the quark's color in SU(3) space. The quantity g_s (or $\alpha_s = \frac{g_s^2}{4\pi}$) is the QCD coupling constant. Besides

quark masses, who have electroweak origin, it is the only fundamental parameter of QCD. Finally, the field tensor $F^A_{\mu\nu}$ is given by

$$F^A_{\mu\nu} = \partial_\mu \mathcal{A}^A_\nu - \partial_\nu \mathcal{A}^A_\mu - g_s f_{ABC} \mathcal{A}^B_\mu \mathcal{A}^C_\nu. \tag{1.6}$$

It is the third 'non-Abelian' term on the right-handside of eq. (1.6) which distinguishes QCD from QED, giving rise to triplet and quartic gluon (gluons transport the color charge and self-interact), self-interactions and ultimately to the property of asymptotic freedom.

1.2.1 Asymptotic freedom and confinement

The restriction of the strong force to subatomic distances is a consequence of two features, *asymptotic freedom* and *color confinement*. Confinement is a necessary requirement to explain the fact that isolated quarks have never been observed in any experiment, although symmetry arguments and scattering experiments in the 1960s established quarks, with $-1/3$ or $+2/3$ units of electric charge and the quantum number, "color charge", as the basic constituents of hadrons [24].

In the interaction between quarks, the force between them becomes smaller the closer they are, this is the asymptotic freedom, at small distances or large momentum scales, the quarks are asymptotically free. This phenomenon implies that in high-energy scatterings, quarks move within hadrons essentially as free, non-interacting particles.
However, at great distances, the force between the quarks becomes so great that it prevents them from being separated; this is known as the color confinement. The intensity of the interaction is determined by the coupling constant. In QCD, the constant is variable (it is variable in quantum field theories), decreasing at high energies and increasing at smaller distances, due to the non-abelian nature of the symmetry group. The latter implies the impossibility of perturbative study of the theory at low energies. Therefore, two analysis approaches are distinguished; since quarks interact weakly at high energies, calculations in perturbation theory are useful on this scale; however, the confinement of quarks and gluons within hadrons is a phenomenon that occurs at low energies, so its study implies non-perturbative QCD tools. One way to solve this is the discretization of space-time to reduce the infinite degrees of freedom to a finite number. This is known as Lattice QCD [5]. In turn, other models can be used to describe this approach, such as the Hydrodynamics model, and the Color String Percolation Model (SPM), which is described later.

1.2.2 Coupling constant

The coupling constant is a variable that determines the intensity of an interaction. Besides the quark masses, the only free parameter of the Lagrangian of QCD is the coupling constant g_s.
The coupling constant itself is not a physical observable, but rather a quantity defined in the context of perturbation theory, which enters into predictions for experimentally measurable observables, and which varies with the energy scale. The image (1.2) shows the summary of measurements for the constant at different energies and the corresponding setting.

In QCD, virtual quark-antiquark pairs appear, which tend to shield color charge, however, the force-carrying particles, gluons, have color charge. Each gluon carries a color charge and a different anti-color charge. The net effect of virtual gluon polarization in a vacuum is not to shield the field, but to increase it and affect its color. Getting closer to a quark lessens the effect of non-shielding of the surrounding virtual gluons; therefore the contribution of this effect is to weaken the color charge of a quark with a decrease in distance.

Since it is sought to have finite terms that can be compared with the observations, the theory must be renormalized. This involves choosing a renormalization scheme that introduces an

arbitrary mass parameter. In order to have an expression similar to QED, we have the coupling constant $\alpha_s = g^2/4\pi$. The running of the coupling constant α_s is determined by the renormalization group equation :

$$Q^2 \frac{\partial \alpha_s}{\partial Q^2} = \beta\left(\alpha_s\right). \tag{1.7}$$

With Q, the energy scale. β, the Callan-Symanzik beta function that has the following perturbative expansion [28]:

$$\frac{da}{d\ln\mu^2} = \beta(a) = -\sum_{n=0}^{\infty} \beta_n a^{n+2}, \quad a = \frac{\alpha_s(\mu)}{4\pi}. \tag{1.8}$$

The first coefficients, and the number of quarks $n_f = 6$:

$$\beta_0 = 11 - \frac{2}{3}n_f, \quad \beta_1 = 102 - \frac{38}{3}n_f, \quad \beta_2 = \frac{2857}{2} - \frac{5033}{18}n_f + \frac{325}{54}n_f^2. \tag{1.9}$$

Perturvative QCD shows us how the coupling constant varies with scale. Referring to the observations of the experiment with the latter. With which, a value for the parameter can be chosen at a reference scale large enough to be in a perturbative domain. An alternative approach, which was adopted historically and is still convenient for many purposes, is to introduce a dimensionful parameter directly into the definition of $\alpha_s\left(Q^2\right)$. Λ represents the scale at which the coupling would diverge, if extrapolated outside the perturbative domain. It indicates the order of magnitude of the scale at which $\alpha_s\left(Q^2\right)$ becomes strong. Its value is in the neighbourhood of 200 MeV. Thus $\alpha_s\left(Q^2\right)$ becomes large, and perturbation theory breaks down, for scales comparable with the masses of the light hadrons. This could be an indication that the confinement of quarks and gluons inside hadrons is actually a consequence of the growth of the coupling at low scales, which is a corollary of the decrease at high scales that leads to asymptotic freedom. The introduction of Λ allows us to write the asymptotic solution for α_s in terms of this parameter. In leading order (LO), retaining only the β_0 coefficient in the β function, we obtain:

$$\alpha_s\left(Q^2\right) = \frac{1}{\beta_0 \ln\left(Q^2/\Lambda^2\right)} \tag{1.10}$$

The definition of Λ is extended to next-to-leading order (NLO) by including also the β_1 coefficient in the integral [29]:

$$\frac{1}{\alpha_s\left(Q^2\right)} + \beta_1 \ln\left(\frac{\beta_1 \alpha_s\left(Q^2\right)}{1 + \beta_1 \alpha_s\left(Q^2\right)}\right) = \beta_0 \ln\left(\frac{Q^2}{\Lambda^2}\right) \tag{1.11}$$

For small distances (high values of Q^2) perturbatives methods can be applied (pQCD), while phenomenological models are used for processes involving at large distances (small Q^2). The behaviour of the QCD coupling constant is mainly due to the presence of auto-interactions of the gauge bosons. The parameter Λ depends on the normalization frame and the number of active flavors (number of quarks with mass $m_q < Q$). So the perturbative approximation fails in scales comparable with the mass of the light hadrons ($Q \sim 1\text{GeV/c}$).

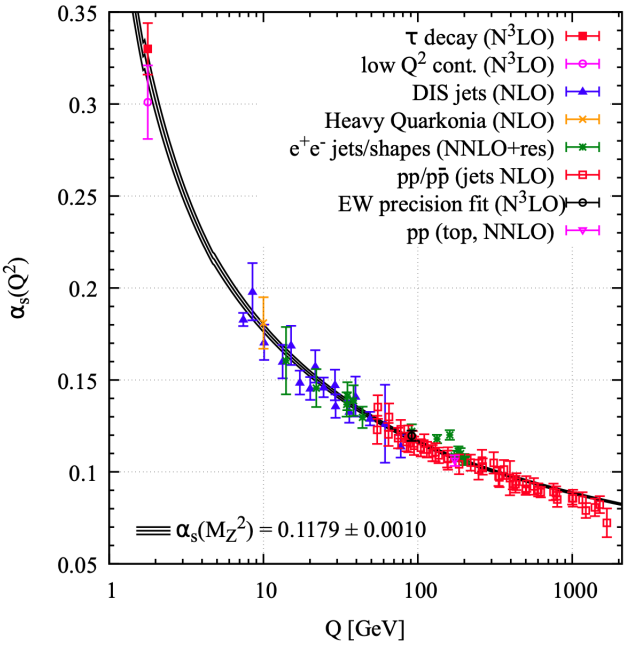

Figure 1.2: Summary of measurements of α_s as a function of the energy scale. The respective degree of QCD perturbation theory used in the extraction of α_s is indicated in brackets (NLO: next-to-leading order; NNLO: next-to-next-to-leading order; NNLO+res.: NNLO matched to a resummed calculation; N^{3}LO : next-to-NNLO) [22].

Chapter 2

Ions Collisions and Quark Gluon Plasma

Observed densities in the universe vary by orders of magnitude, from 10^{-6} nucleons/ cm^3 on average in the Universe, to 10^{38} nucleons/ cm^3 inside the core of a neutron star [30]. At conditions of high density and temperature, the individual hadrons lose their boundary and matter is best described in terms of its components: quarks and gluons, commonly called Quark-Gluon Plasma (QGP).
In 1979, Leonard Susskind [2] studied the confinement of quarks at finite temperature in lattice QCD and found that the confinement is strictly a low-temperature phenomenon. A transition to a plasma-like phase occurs at high temperatures.

In this field, there have been several experimental efforts to observe such a phase, including the Alternating Gradient Synchrotron (AGS) at the Brookhaven National Laboratory (BNL) and the Super Proton Synchrotron (SPS) at the European Organization for Nuclear Research (CERN). Both facilities accelerated proton beams and various types of ions. Specifically, the AGS accelerated Si and Au, while the SPS accelerated O, S, Pb, and proton-proton (pp) and proton-nuclei ($p + A$) collisions. The maximum possible energy of the center of mass for those fixed target experiments was quite low, 4.4 GeV/nucleon for Au+Au collisions in the AGS and 16.8 GeV/nucleon for the Pb+Pb collisions in the SPS [31].
Today, there are two heavy-ion nuclear colliders where both the projectile and the target particles are accelerated, enabling the generation of significantly higher energies compared to fixed-target installations. The Relativistic Heavy Ion Collider (RHIC) at BNL and the Large Hadron Collider (LHC) at CERN facilitate heavy collisions, (gold and lead, primarily), achieving energies up to 200 GeV/nucleon and 2.56 TeV/nucleon (for Run2), respectively, at the center of mass. These exceptionally high energies, surpassing the production threshold for most particles, allow for the study of rare particle production that remains inaccessible in lower-energy facilities [32].

2.1 Phase Diagram in Nuclear Matter

Based on lattice QCD studies, there is a change in the state of matter (a phase transition) from a hadronic system to a nearly free gas of quarks and gluons, the quark-gluon plasma. The quark matter phase can be reached either by compressing nuclear matter to high densities while at rather low temperatures (along the baryon density axis) or by heating the vacuum (along the temperature

axis). The high density phases are expected to play a key role in the interior of neutron stars. On the other hand, the high temperature, heated-vacuum quark-matter phase was first produced in nature at the Big Bang. Phase transitions in nuclear matter also involve symmetries. In the early universe, the quarks were massless and there were an equal number of quarks and antiquarks. In the universe today, after the transition to normal nuclear matter, there is a small difference in the up and down quark masses – as well as an even larger difference between the light quark masses and those of the other quarks, even between the light quarks and the strange quark. This mass difference is caused by chiral symmetry breaking [31]. At high temperatures chiral symmetry is expected to be restored. Today's universe is baryon dominated with quarks bound into normal matter while antibaryons do not exist in nature and must be produced in the laboratory. We expect that in heavy-ion collisions, there should be an equal number of quarks and antiquarks produced in the central rapidity region.

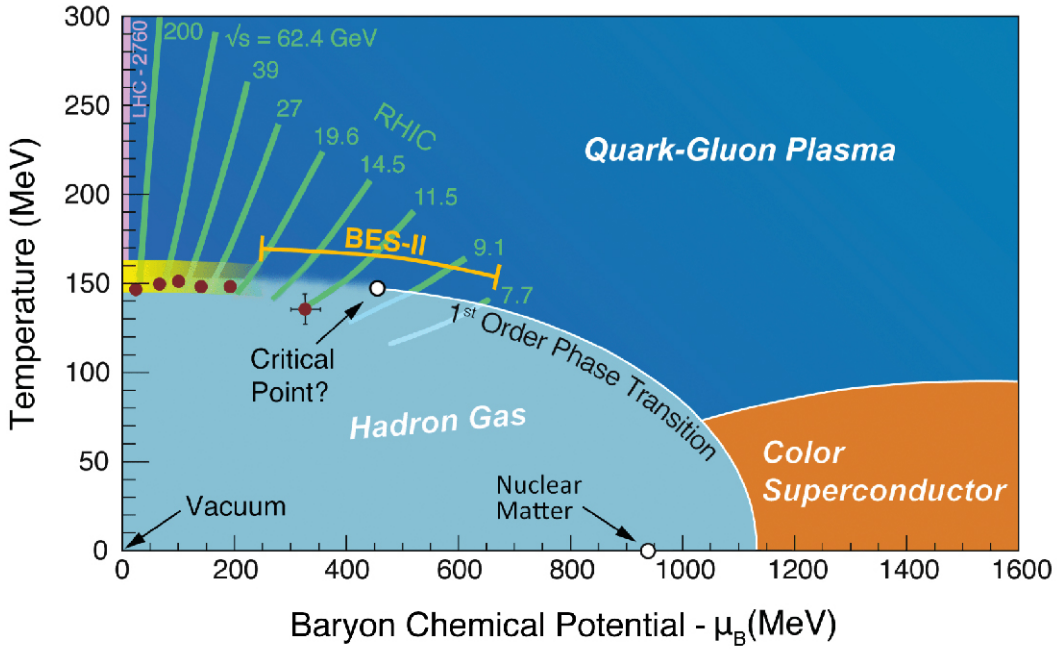

Figure 2.1: Phase diagram in Quark Matter [33].

We are currently looking for the best description of the system, which implies having a phase diagram in QCD as detailed as possible and a better characterization of the QGP.

2.2 Standard Heavy Ion Collision Model

Historically, T.D. Lee, in collaboration with G.C. Wick, were the first to speculate on an abnormal nuclear state in which the mass of the nucleon is zero or close to zero in an extended volume and non-zero outside the volume [2, 3]. They also suggested that an effective way to search for these new objects was through high-energy heavy ion collisions.
Relativistic heavy ion collisions are a unique tool to create and study hot QCD matter and its phase transition under controlled conditions. As in the early universe, a hot, dense system is created in a

collision of heavy ions, which expands and cools. During this evolution, the system probes a range of energy densities and temperatures, and possibly different phases. Whenever quarks and gluons undergo multiple interactions, the system will thermalize and form the QGP which subsequently undergoes collective expansion and eventually becomes so dilute that it hadronizes. This collective expansion is called eliptic flow.
In 2001, the first results from the RHIC program indicated that in Au + Au head-on collisions at 200 GeV per nucleon pair, most of the energy is deposited in a medium whose expansion is well described hydrodynamically, that is, as a flowing fluid. The hydrodynamic nature of matter was ultimately quantified in terms of *shear viscosity*, which happens to approximate the smallest possible conjectured ratio of viscosity to entropy density $[\eta/s \geq \hbar/(4\pi k_{\mathrm{B}}) = 1/4\pi]$ of any fluid [34].
This nuclear matter has an initial temperature of the order of 350-400 MeV, or equivalently four trillion Kelvin, and as such is composed of quarks and gluons no longer bound to neutral-colored hadrons such as protons and neutrons. Subsequent measurements of Pb + Pb collisions at the LHC were up to 5.02 TeV per nucleon pair showing similar fluidity with matter from a higher initial temperature of the order of 400 to 600 MeV. In both cases, the collisions Au + Au and Pb + Pb create a QGP that behaves like an almost perfect fluid, that is, a fluid with $\eta/s \sim 1/4\pi$. Thus, a theory has been developed within the paradigm of the *Big Bang*, *Little Bang*, as a standard model for the temporal evolution of heavy ion collisions, with the following phases:

1. Highly contracted nuclei collide with a very short travel time ($\ll 1fm/c$). Predominantly through gluon interactions in the nuclei, often described in terms of gluon fields, energy is deposited in the newly created medium. The initial distribution of the energy deposited in the transverse plane perpendicular to the direction of the beam and inhomogeneous is called the initial condition.

2. Matter is initially out of equilibrium and some time is required for it to equilibrate. During this time, matter expands at almost the speed of light in the longitudinal direction and begins to expand radially in the transverse plane. This is often known as the pre-equilibrium stage.

3. When matter is nearly in equilibrium, it is modeled by viscous hydrodynamics using an equation of state from *Lattice QCD* calculations.

4. The fluid is cooled to a temperature corresponding to the QGP crossing transition T $\approx$ 170 MeV (determined by the inflection point of the Polyakov loop, roughly equivalent to the confinement-deconfinement transition) and then breaks up into hadrons.

5. The resulting hadrons scatter, both inelastically, until what is called chemical freeze-out, and elastically, until kinetic freeze-out, at which time they are assigned their final-state momenta as measured experimentally.

Computer simulations of a large number of individual collisions follow each of these stages up to the final hadron predictions that are measured experimentally. The matter produced in the collision is subject to enormous longitudinal pressure, expanding at almost the speed of light in this direction, highlighting features such as:

- There is a general pattern of strong radial outward expansion with the highest volume velocity near the periphery reaching 75% of the speed of light.

- Heavier hadrons receive a larger momentum change that can be measured as a distinctive feature in the distribution of transverse momentum of hadrons as a function of their mass.

- The spatial distribution of the matter and its temperature profile are lumpy, despite the lumpiness of the initial condition already having been washed out to some degree by viscous effects. These inhomogeneities lead to substantial distortions in the azimuthal distribution of particles, which are quantified in terms of a Fourier expansion as:

$$\frac{\mathrm{d}n}{\mathrm{d}\phi} \propto 1 + \sum_n 2v_n\left(p_T\right)\cos\left[n\left(\phi - \Psi_n\right)\right], \tag{2.1}$$

  where p_T and ϕ are the transverse momentum and azimuthal angle of each particle and Ψ_n is the overall orientation of the nth moment. The first four moments, v_1, v_2, v_3, and v_4, are often referred to as directed, elliptic, triangular, and quadrangular flow coefficients, respectively. Near midrapidity, for semicentral collisions, the dominant Fourier coefficient is v_2, reflecting the efficient hydrodynamic translation via pressure gradients of the initial almond-shaped overlap region to momentum space. Again, because of the larger fluid velocities built up along directions of steeper pressure gradients, heavier hadrons will have their flow patterns $v_n\left(p_T\right)$ shifted outward in p_T.

Hydrodynamic calculations describe the measured higher-order coefficients v_3 to v_5 . Such comparisons constrain both the initial inhomogeneities that are the source of the fluid anisotropies and the medium properties such as the shear viscosity, which has a larger damping effect on the higher-order coefficients. There is a nice analogy between these v_n measurements in heavy ion physics reflecting the initial spatial anisotropies and the spherical harmonic moment measurements from the cosmic microwave background reflecting the earlier inhomogeneities in the early Universe, providing key constraints on QGP properties from the former and early Universe properties from the latter. Other important observable is the jet quenching. Jet quenching is the suppression of high–transverse momentum particle and/or jet production relative to yields expected from the number of hard scatters in a collision. Jet quenching studies give us a wealth of information on both how the medium responds when a high-energy quark or gluon jet produced in an initial hard scattering traverses it, and how a fast quark or gluon jet is modified by the medium as it passes through it. The standard model of $A + A$ collisions has now been well established and tested with great precision. This model describes a multitude of experimental measurements including the mass dependent p_T spectra, the v_n flow coefficients, the distribution of event-by-event fluctuations in those flow coefficients, multiparticle correlations referred to as cumulants [34].

2.2.1 Small Systems

The small systems are referred to less density systems as pp or pPB collisions. Measurements in $d + Au$ and pPb collisions at RHIC and the LHC have been very useful, for example, in constraining nuclear modified parton distribution functions (nPDFs) that determine the initial gluon distributions that determine the first epoch of heavy ion collisions. However, in 2010, the CMS Collaboration examined ultrahigh- multiplicity pp collisions at the LHC and found that particles had a weak, though clear, preference to be emitted along a common transverse ϕ angle across all rapidities [34]. Then, in 2012, p+Pb data taking at the LHC, quickly followed by a reexamination of d +Au data at RHIC, revealed that most of the signatures for hydrodynamic flow in A + A collisions also existed in these smaller systems. The firsts studies beby these small system measurements, and the attempt to reconcile them in the context of the heavy ion standard model.

In $A + A$ collisions, an important confirmation of the heavy ion standard model comes from the energy loss of high- p_T partons traversing the medium, referred to as jet quenching. Jet quenching models calculate the rate and kinematics for hard scattering, that is, large momentum-transfer interactions, and then propagate the resulting partons through the spacetime evolution of the matter calculated from hydrodynamic codes. Jet quenching was discovered at RHIC in

Au + Au collisions as a factor-of-five suppression of high- p_T hadrons relative to their expected rate from scaling up $p + p$ yields. A critical observation made in 2003 was that this quenching effect disappeared in $d+$ Au collisions where no dense medium was expected. No suppression was observed in $d+$ Au collisions; thus, at the time, jet quenching was confirmed as an exclusively final-state effect from the medium in $A + A$ collisions. Similar measurements at the LHC of single hadrons in PbPb and pPb collisions demonstrate the quenching observed in $A + A$ collisions is not observed in small systems [33]. The jet quenching effect in $A+A$ collisions becomes more prominent in more central, higher-multiplicity reactions as the average in-medium path the partons traverse correspondingly grows. In small systems, the medium created is smaller, so the average path is expected to be significantly shorter. One possibility is that after the hard scattering the parton is in a highly virtual state, and its evolution may be only modestly affected by scattering with other partons in the medium.

Chapter 3

Color String Percolation Model

In the 1970s, there was interest in the behavior of matter at high density and/or high temperature, given the possibility of distributing high energy or high nucleon density in a large volume to temporarily restore broken symmetries of the physical vacuum by creating abnormal dense states. of nuclear matter [2]. Subsequently, it was pointed out that the asymptotic freedom in QCD implies the existence of a high-density matter, formed by unconfined quarks and gluons. This phase of quarks and gluons was named Quark-Gluon Plasma (QGP) [35].
Due to the nature of the strong interaction, it is necessary to employ non-perturbative methods to study phase transition phenomena, such as hadron formation and confinement effects.
One model for studying phase transitions is the Color String Percolation Model (CSPM), which is derived from percolation theory. Majority of the models based in percolation roughly coincide in basic postulates such as the number of strings and its dependence on energy and centrality, which is taken from the Glauber-Gribov model [35].

3.1 Percolation Theory

In color string percolation, particle production is described in terms of color strings stretched along the line connecting the partons of the projectiles in collisions of heavy ions (or proton bunches). These strings decay into pairs of (q-$\bar{q}$) and (qq-$\overline{qq}$), forming new strings.Due to confinement, the color of these strings is limited to a small area $S_1 = \pi r_0^2$, with $r_0 = 0.2$ fm in transversal space [35].
In CSPM strings have a finite area in the transverse space in terms of the color field. The area is restricted to a finite disc of a given radius dictated by confinement. When the string with radii r_0 and string density ξ are uniformly distributed on the much larger transverse nuclear collision area S_N they may overlap. ξ is given by $N_s S_1/S_N$ where the single disc area is S_1 and S_N is the total number of strings. Color strings may be viewed as small areas in the transverse plane filled with color field created by colliding partons. As the collision energy or the size and centrality of the system increase, the number of strings grows, and they start to overlap, forming clusters, in the transverse plane. At a certain critical density $\xi_c = 1.2$ a macroscopic percolation cluster appears, very similar to disks in the two-dimensional percolation theory. That marks the percolation phase transition [11–13]. This percolating cluster of color strings is considered equivalent to the partonic deconfinement state of matter. Subsequently, the strings hadronize through the interaction between partons, following the Schwinger mechanism, generating the observed hadrons in the final state.

In string percolation, the basic objects are strings, and it is necessary to know their number, rate of extension, fragmentation, and number distribution. String percolation is not directly derived from QCD and is based on string color exchange models.

The model has two-dimensional percolation as a paradigm: small disks of area πr_0^2 are randomly distributed over a large surface, allowing them to overlap each other. As the number of disks increases, overlapping disk clusters begin to form.

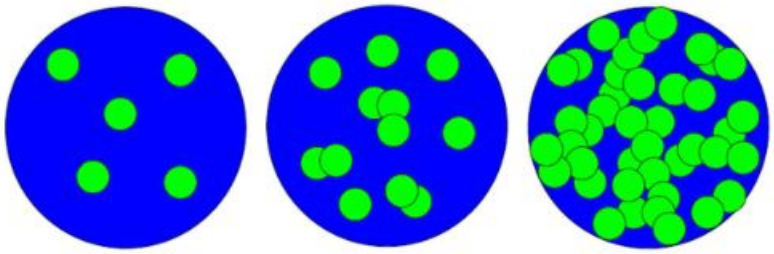

Figure 3.1: From left to right: isolated disks, cumulus formation, percolation [35].

Given N disks, the density of the disk is defined as $\xi = N/S$, where S is the surface area. The average size of clusters increases with, ρ, and at a certain critical value ρ_c, the cluster encompasses the entire surface. If this critical point is considered the equivalent to the thermodynamic critical point that describes a phase transition, in this sense, the geometric phase transition will give rise to a connected system that is considered the equivalent of the phase change in a thermodynamic system, precisely it is the region where the systems considered in this work are studied, close to the QGP. The critical density for the start of continuous percolation has been determined by numerical simulations for different systems, which in the two-dimensional disc case is obtained between $1.12 - 1.17$ [36]. This parameter varies according to the surface and whether or not it is homogeneous.

3.2 String Percolation

The production of multiple particles at high energies can be described in terms of colored strings stretched between projectile and target.
Hadronization of these strings produces the observed hadrons. The basic characteristic feature of the color string model is that the strings have a finite area in transverse space. In terms of the gluon color field they can be thought of as the flow of color tubes stretched between the colliding partons, which in transverse space are restricted to a finite disk of a given radius, dictated by the connector. The particle creation mechanism is then similar to the Schwinger mechanism; creation of pairs in a constant electric field that covers all space; except that now space is finite in the transverse plane. At low energies for the collision of hadrons and nuclei with relatively small atomic numbers the fact that the chains have finite dimension has no influence on the results. In the transverse plane, the strings project as disks over great distances from each other and the creation of particles is not affected by their interaction.
However, with increasing energy and/or atomic number of colliding particles, and the centrality, the number of strings increases. Once the strings have a certain dimension in transverse space they begin to overlap forming clumps, similar to the disks in the two-dimensional percolation theory.

The geometric behavior of the strings in the transverse plane then follows the disk percolation. In particular, at a certain critical string density, a macroscopic cluster appears (infinitely in the thermodynamic limit), marking the percolation phase transition. The disk density is expressed as:

$$\xi^t = \frac{S_1}{S_n} N_s. \tag{3.1}$$

Where S_1 is the cross-sectional area of a single string, S_n is the area of interaction that behaves like a single color source with a color field larger and N_s is the number of strings created in the collision. In the case of having completely central collisions, in collisions of pp, S_n will be the cross-sectional area of a proton, resulting in a density of strings:

$$\xi^t = \left(\frac{r_0}{R_p}\right)^2 N_s. \tag{3.2}$$

With, $r_0 = 0.25$ fm is the radius of a single string and R_p= 1 fm, the radius of a proton. A cluster of n strings behaves like a single string with energy and moment corresponding to those of the vectorial sum of color and moment of the individual strings that compose it. In this sense, the multiplicity μ and the average square transverse momentum $\langle p_T^2 \rangle_n$ of the particles produced in a cluster is given by:

$$\mu_n = \sqrt{\frac{nS_n}{S_1}} \mu_1. \tag{3.3}$$

Where μ_1 and $\langle p_T^2 \rangle_1$ are the multiplicity and mean square transverse moment, respectively, of a single string.

$$\langle p_T^2 \rangle_n = \sqrt{\frac{nS_1}{S_n}} \langle p_T^2 \rangle_1 . \tag{3.4}$$

The process of generating strings at a certain density suppresses the creation of more strings, so the multiplicity $\frac{dN}{dy}$, or the number of particles, in the region of central speed ($\eta \simeq y$), can be scaled with the number of strings [35]. The scaling function is introduced to relate the multiplicity and the average number of strings:

$$\frac{dN}{dy} = kF\left(\xi^t\right) N^s. \tag{3.5}$$

With k a normalization factor to determine the percentage of centrality. The scaling function that best fits the string density parameter is the following:

$$F\left(\xi^t\right) = \sqrt{\frac{1 - e^{-\xi^t}}{\xi^t}}. \tag{3.6}$$

Recent studies [37] have applied numerical techniques to find more efficient combinations, like:

$$F_s\left(\xi\right) = A\sqrt{\frac{1 - e^{-\xi}}{\xi}} + B\sqrt{\frac{1 + e^{-\xi}}{\xi}} \tag{3.7}$$

The coefficients found in , are the following and are compared in the analysis section

$$A = 0.7715 \pm 0.0122 \tag{3.8}$$

$$B = 0.0609 \pm 0.0062. \tag{3.9}$$

For pp collisions, the average number of strings defined in the area of interaction is an energy-dependent quantity:

$$\bar{N}^s = 2 + 4\left(\frac{S_1}{S_n}\right)\left(\frac{\sqrt{s}}{m_p}\right)^{2\lambda} \tag{3.10}$$

where $m_p = 938.3$ MeV is the mass of the proton, and the exponent λ describes the increase of multiplicity with energy in p-p and A-A collisions [38]. To determine μ_0 and λ, equation **??** is used with experimental data of multiplicity:

$$\mu = \mu_0 \bar{N}^s F(\xi), \tag{3.11}$$

introducing the energy dependence of the center-of-mass energy of collisions through equations **??**, **??**, **??**. A first fit with $S = \pi R_p^2$, where $R_p = 1$ fm is the radius of the proton, provided the values of 0.63 and 0.201 for μ_0 and λ, respectively [38]. In addition, for the determination of the density of strings of form experimentally, the invariant transverse momentum spectrum is used in the manner described by a power law:

$$\frac{1}{N}\frac{d^2N}{dp_T^2} = \frac{(\alpha-1)(\alpha-2)}{2\pi p_0^2}\frac{p_0^\alpha}{[p_0+p_T]^\alpha}. \tag{3.12}$$

Where p_0 and a are energy dependent parameters. Where it is obtained from:

$$\frac{1}{N}\frac{d^2N}{d\eta dp_T} = \frac{a\left(p_0\sqrt{\frac{F\left(\xi_{pp}^t\right)}{F\left(\xi_{HM}^t\right)}}\right)^{\alpha-2}}{\left[p_0\sqrt{\frac{F\left(\xi_{Pp}^t\right)}{F\left(\xi_{HM}^t\right)}}\right)+p_T\Bigg]^{\alpha-1}} \tag{3.13}$$

Where ξ_{HM} corresponds to the events of high multiplicity and ξ_{pp} to those of minimum bias, that is, to the most general distributions in terms of multiplicity. So a first consideration is to adjust the spectrum of minimum bias:

$$\frac{1}{N}\frac{d^2N}{d\eta dp_T} = \frac{a\left(p_0\beta\right)^{\alpha-2}}{\left(p_0\beta+p_T\right)^{\alpha-1}}, \quad \text{with} \quad \beta \to \sqrt{\frac{F(\xi_{pp})}{F(\xi_{HM})}}, \tag{3.14}$$

The constants are variables of the energy scale and therefore must be determined by adjusting to the different multiplicity values of the charged particle spectra, taking the central values of the parameters given by the first adjustment and the color reduction factor obtained from the number of strings from the setting [39].

3.2.1 Thermodynamics

The tension of the strings in macroscopic clusters fluctuates around its mean value due to fluctuations of the chromo-electric field coming from the nature of the quantum vacuum in QCD. These fluctuations determine an exponential distribution, in terms of the color reduction factor that is related to a thermal distribution [40]:

$$\frac{dN}{dp_T^2} \sim \exp\left(-p_T\sqrt{\frac{2F(\xi)}{\langle p_T^2\rangle_0}}\right). \tag{3.15}$$

The average temperature of the system is proportional to the average moment of the particles produced, in this way a local temperature is defined, even in small systems, which in terms of the model is expressed as:

$$T(\xi) = \sqrt{\frac{\langle p_T^2 \rangle_0}{2F(\xi)}}. \tag{3.16}$$

The fit made to the transverse momentum distributions provide the average temperature described by 3.16, where $\sqrt{\langle p_T^2 \rangle_0}$=190.25 MeV is obtained from the result of the HOTLQCD collaboration for the critical temperature [41].

Chapter 4

Thermodynamics and Tsallis Distribution

The most studied observables in high-energy particle collisions are the transverse momentum distributions of identified hadrons. Over several decades of study, the thermal description has achieved significant accomplishments, such as the assumption that particles in the final state originate from a system in thermal and chemical equilibrium in the hadronic phase.

According to Boltzmann-Gibbs statistics, in this model, the hadron spectra are described by exponential distributions in the form:

$$f(E) \sim \exp\left(-\frac{E-\mu}{T}\right) \tag{4.1}$$

where μ is the chemical potential and T is an associated temperature. However, exponential fits fail in the moderate and high p_T regime ($p_T > 3$ GeV). This was attributed to the assumption that in this regime, hadron production is governed by non-thermal and out-of-equilibrium perturbative QCD processes, which are physically different.

An advance in describing this scenario was originally formulated over three decades ago as an attempt to generalize the Boltzmann-Gibbs theory. Although the theory has many far-reaching consequences, its essence can be understood by using a particular generalization of the exponential and logarithm functions:

$$\exp_q(x) = [1 + (1-q)x]^{1/(1-q)} \tag{4.2}$$

$$\ln_q(x) = \frac{x^{1-q} - 1}{1-q} \tag{4.3}$$

The development of the approach to high-energy physics demands thermodynamic consistency, prescribing the first law of thermodynamics with a first-order Euler equation:

$$P = Ts + \mu n - \varepsilon \tag{4.4}$$

Together with:

$$\begin{aligned} &P = -\left.\tfrac{\partial\Omega}{\partial V}\right|_{T,\mu} = -\tfrac{\Omega}{V}, \quad n = \left.\tfrac{\partial P}{\partial \mu}\right|_{T,V}, \quad s = \left.\tfrac{\partial P}{\partial T}\right|_{V,\mu} \\ &\varepsilon = T\tfrac{\partial P}{\partial T} + \mu\tfrac{\partial P}{\partial \mu} - P, \quad N = \tfrac{\partial\Omega}{\partial V}, \quad S = \tfrac{\partial\Omega}{\partial T} \end{aligned} \tag{4.5}$$

The grand canonical potential:

$$\Omega(T, V, \mu) = -T \ln \mathcal{Z} \tag{4.6}$$

Considering homogeneity in space:

$$\ln \mathcal{Z} = V \int \frac{\mathrm{d}^3 p}{(2\pi)^3} f\left(\frac{E-\mu}{T}\right) \tag{4.7}$$

Distributions with the form given in equation (4.2) are generally called Tsallis or Tsallis-Pareto distributions, named after Constantino Tsallis and Vilfredo Pareto [42]. They have a distinctive property that makes them suitable for studying transverse momentum distributions of hadrons: they describe both the low and high p_T limits simultaneously. In the past two decades, numerous studies have investigated this fact both theoretically and experimentally [43].

Assuming the function to be Tsallis-Pareto, which is associated with equation (4.1) instead of the conventional Boltzmann-Gibbs distribution:

$$f\left(E, q, T_q, \mu\right) = \left[1 + \frac{q-1}{T_q}(E-\mu)\right]^{-\frac{1}{q-1}} \tag{4.8}$$

And with the thermodynamic relation:

$$N = nV = gV \int \frac{\mathrm{d}^3 p}{(2\pi)^3} f^q \tag{4.9}$$

An expression for the invariant transverse momentum distribution is obtained:

$$E\frac{\mathrm{d}^3 N}{\mathrm{d}p^3} = \frac{\mathrm{d}^2 N}{p_T \mathrm{d}p_T \mathrm{d}y \mathrm{d}\phi} = gV \cdot E \cdot f^q \tag{4.10}$$

If $E = p_T$

$$\frac{\mathrm{d}^2 N}{2\pi p_T \mathrm{d}p_T \mathrm{d}y} = A m_T \left[1 + \frac{q-1}{T}\left(p_T\right)\right]^{-\frac{q}{q-1}} \tag{4.11}$$

This distribution has 3 free parameters, T, A, and q. The parameter T is associated with the system temperature, while the parameter q governs the degree of non-thermalization.

Chapter 5

Analysis and Results

Light hadrons are the most abundant particles produced in collisions between heavy ions and pp. The transverse momentum spectra (p_T) of the hadrons can be used to infer the mechanism of particle production in pp collisions. In particle collision experiments, attempts are made to understand the thermodynamic properties of strongly interacting systems. Due to the nature of the collision, the fluid immediately after the collision constitutes a unbalanced system. It is known that fluctuations in the initial conditions lead to specific structures in the final hadronic spectra. Most of these are number density fluctuations, although hot and cold spots are known to arise in rotating fluid, temperature fluctuations are difficult to study experimentally. This has led to most efforts being concentrated only on density fluctuations while analyzing the fluid dynamics of the system. Temperature fluctuations can help to understand various thermodynamic properties of a system. The temporal evolution of these temperature fluctuations has been studied as smaller subsystems.

5.1 Analysis

A comparison is made between the temperature functions in function of multiplicity classes, associated with the models proposed by equations ,3.14 and 4.11.
For the model CSPM, the equation was fitted to the minimun bias distribution of transverse momentum of pion production at different energies in collisions pp, pPb and $PbPb$ to obtain the parameters of the equation 3.14. The equation 3.14 describes the behavior of the minimum bias transverse momentum distributions in a specific region of low transverse momentum, and it is used to fit experimental data to the energies in Table 5.1. This fit is shown in Figure 5.1. The parameters obteined with the minimun bias data are the folllowing:

	$\sqrt{s}$ (TeV)	a	p_0	α	χ^2/ndf
pp	0.9	23.69 ± 2.53	1.86 ± 0.31	9.56 ± 1.01	1.672/13
	2.76	22.55 ± 2.29	1.549 ± 0.25	7.96 ± 0.79	1.755/13
	7	32.29 ± 4.80	1.54 ± 0.25	9.56 ± 1.30	5.28/13
	13	20.3 ± 4.15	1.39 ± 0.43	6.92 ± 1.23	0.2489/13
pPb	5.02	123.18 ± 40.68	4.40 ± 1.68	14.04 ± 4.26	1.892/13
PbPb	2.76	1161.98 ± 682.07	1.21 ± 1.61	8.39 ± 6.14	0.2472 /11
	5.02	6870.90 ± 166649	39.07 ± 96.13	90.53 ± 216.21	0.2489/13

Table 5.1: Parameters CSPM Minumun Bias.

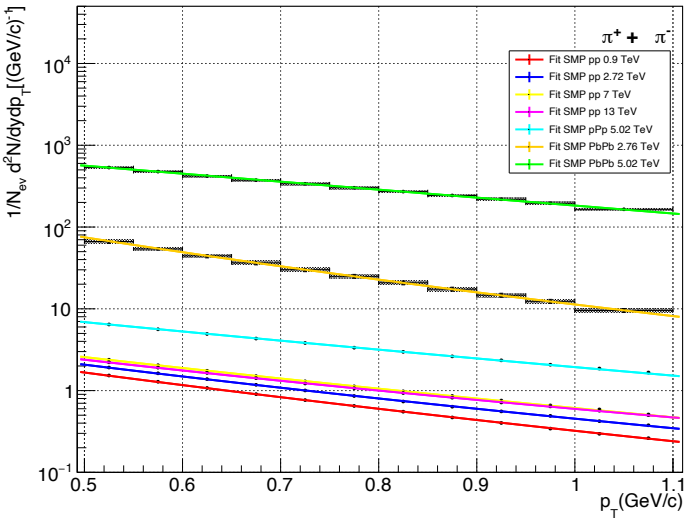

Figure 5.1: Fit to the transverse moment distributions of pions in the range 0.4 GeV $< p_T <$ 1.2 GeV with data of [44], [45], [46], [47], [48].

The fits are presented for the production of pions by the proportion that they represent of the total production. Afterwards, the fit is made to the different multiplicities, as can be seen in the figure:

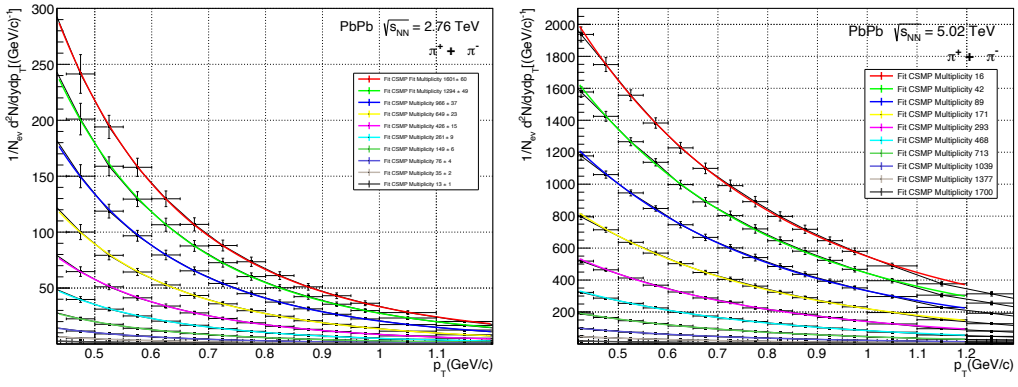

Figure 5.2: Fit to the transverse moment distributions of pions of *pPb* and *PbPb* collisions in the range 0.4 GeV $<p_T<$ 1.2 GeV with data of [46].

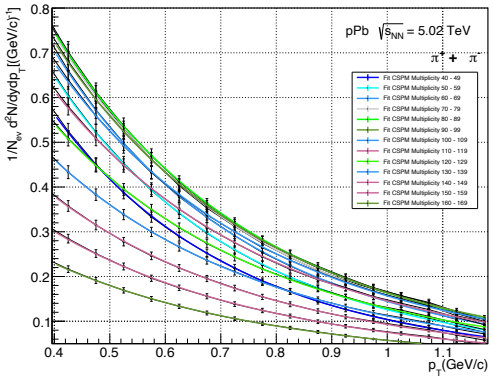

Figure 5.3: Fit to the transverse moment distributions of pions of pPb collisions in the range 0.4 GeV $< p_T <$ 1.2 GeV with data of [46], [47], [48].

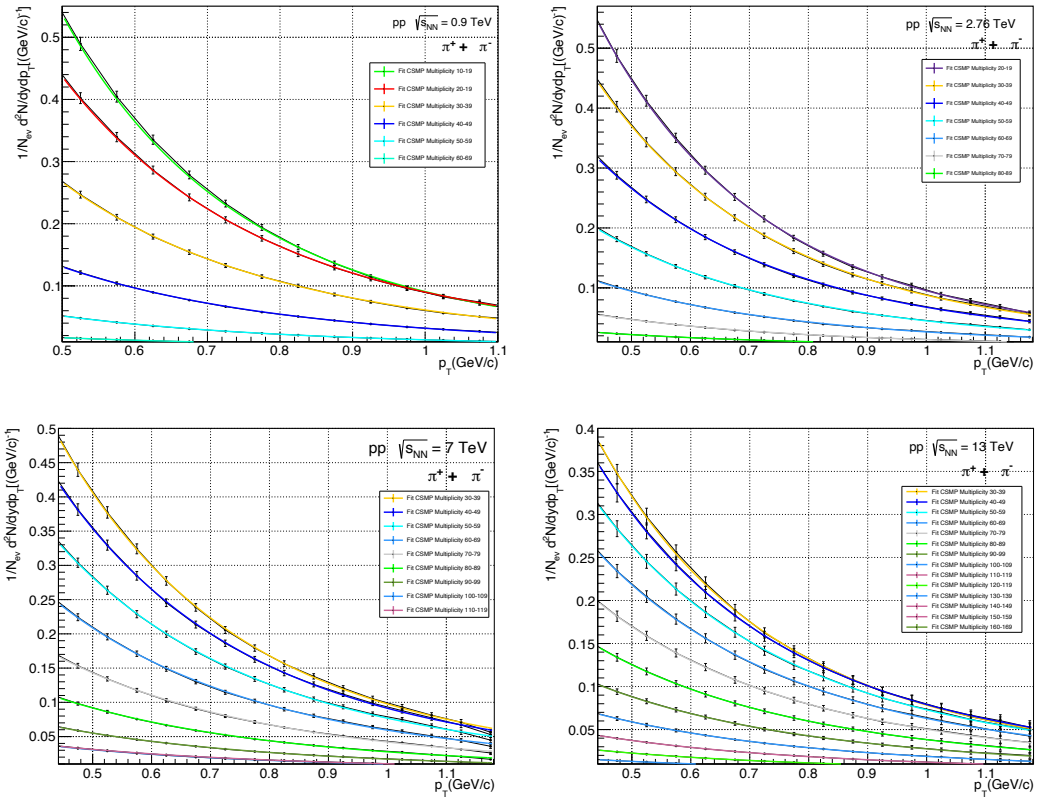

Figure 5.4: Fit to the transverse moment distributions of pions of pp collisions in the range 0.4 GeV $< p_T <$ 1.2 GeV with data of [44], [45].

In the same way, the fit is made for the Tsallis distribution, represented in the equation 4.11:

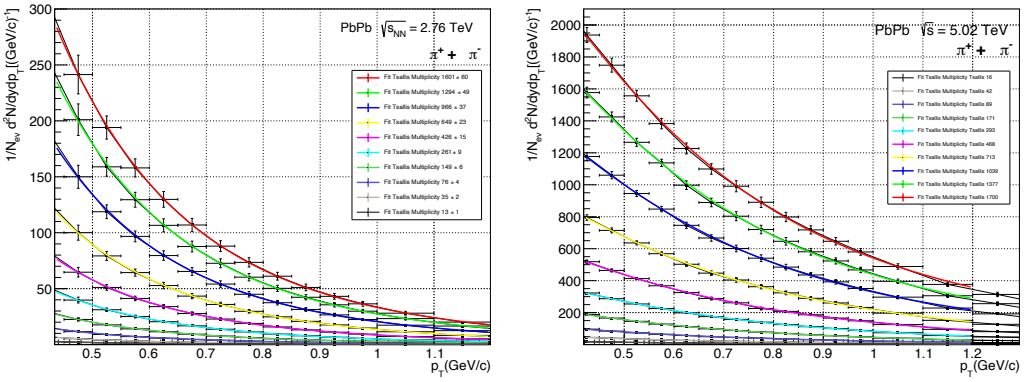

Figure 5.5: Fit to the transverse moment distributions of pions of pPb and $PbPb$ collisions in the range 0.4 GeV $p_T <$ 1.2 GeV with data of [46], [47], [48].

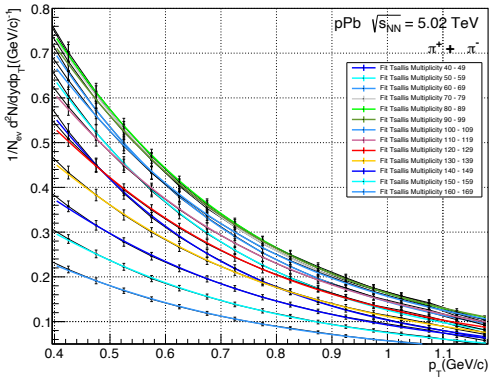

Figure 5.6: Fit to the transverse moment distributions of pions of pPb collisions in the range 0.4 GeV $p_T <$ 1.2 GeV with data of [46].

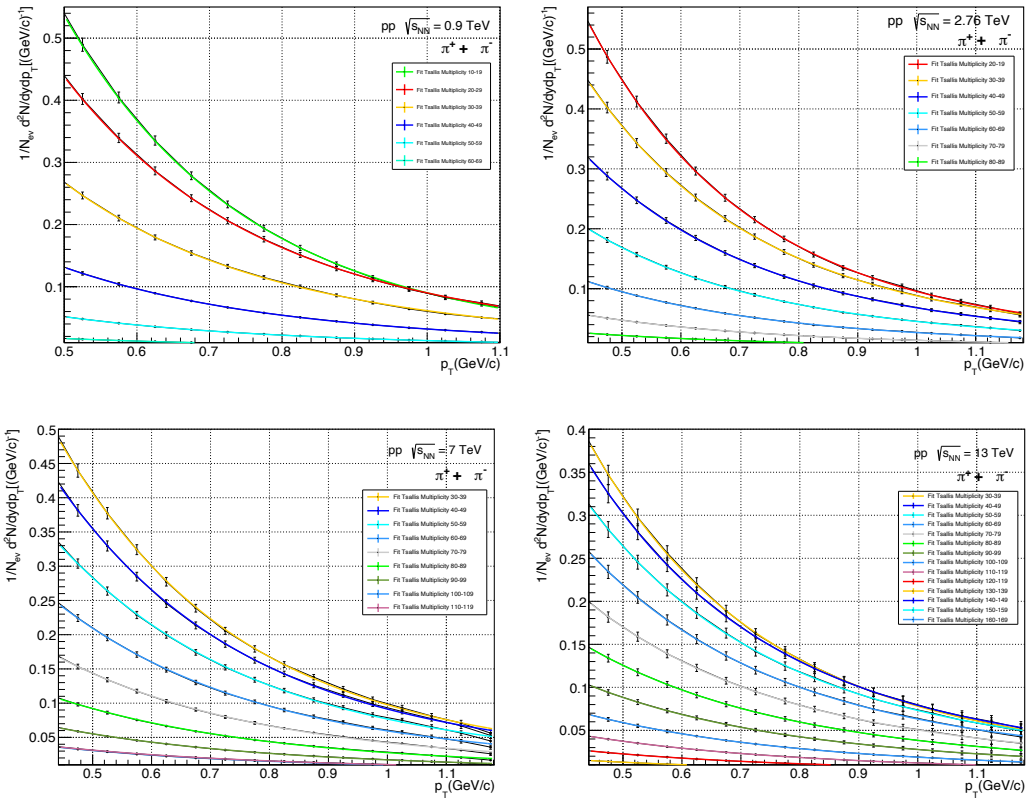

Figure 5.7: Fit to the transverse moment distributions of pions of *pp* collisions in the range 0.4 GeV $< p_T <$ 1.2 GeV with data of [44], [45].

5.1.1 Global temperature

Since we can know the average local temperature with the equation 3.16 in the CSMP,

$$T(\xi) = \sqrt{\frac{\langle p_T^2 \rangle_0}{2F(\xi)}}, \tag{5.1}$$

and the free parameter in the equation 4.11 of Tsallis distribution; we can compute for each energy. Also, is analyzed for the modification presented in 3.7.

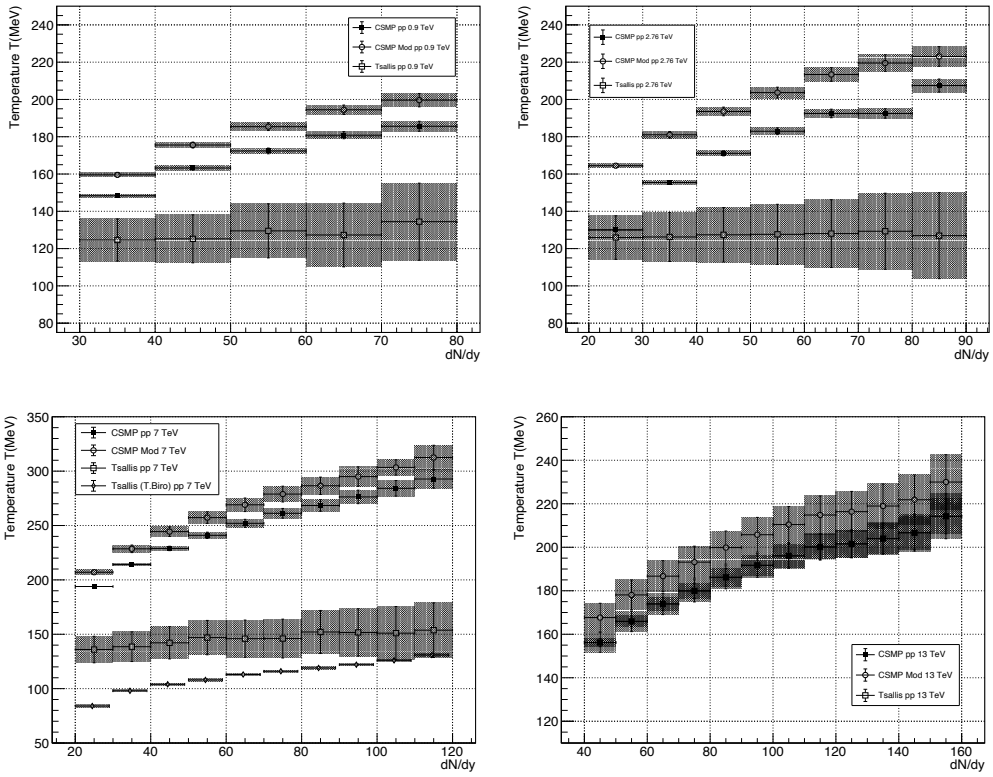

Figure 5.8: Global temperature in CSPM and Tsalllis distribution associated to *pp* collisions.

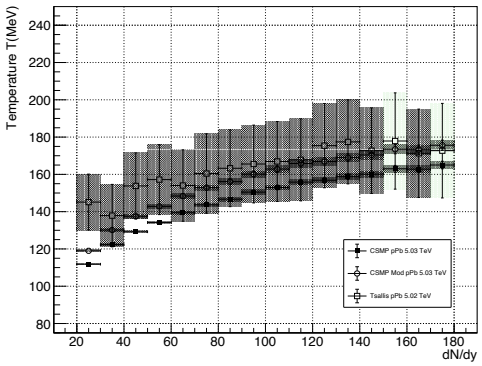

Figure 5.9: Global temperature in CSPM and Tsalllis distribution associated to *pPb* collisions.

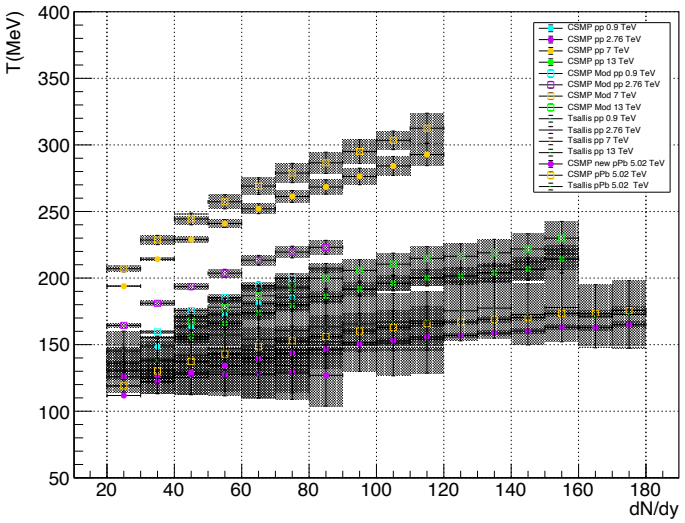

Figure 5.10: Temperature parameter for CSPM ans Tsallis distribution in pp and pPB collisions.

5.1.2 Temperature Fluctuation

The temperature variation (Var) associated with each temperature parameter found for the explored models was calculated with:

$$Var = \frac{T(dy/dn) - < T(dy/dn) >}{< T(dy/dn) >} \tag{5.2}$$

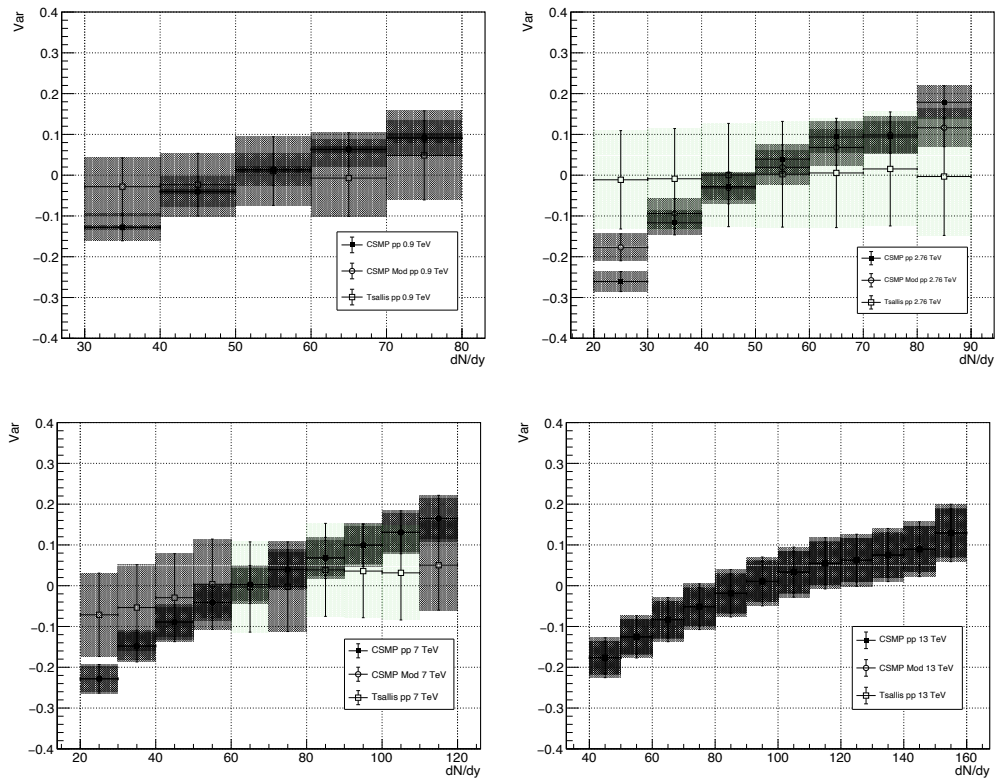

Figure 5.11: Temperature fluctuations associated in *pp* collisions.

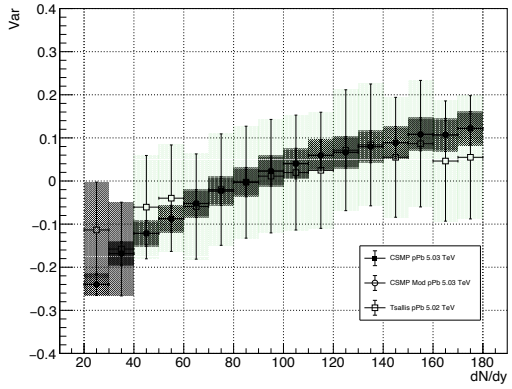

Figure 5.12: Temperature fluctuations associated in *pPb* collisions.

The temperature fluctuations associated with each temperature parameter in the models is calculated with the equation:

$$\nu_T = \sqrt{\sum \frac{1}{N_{class}} \frac{(T(dn/dy) - < T(dn/dy) >)^2}{< T(dn/dy) >}}. \tag{5.3}$$

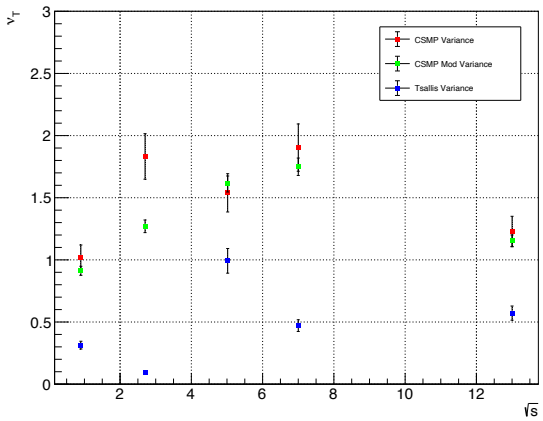

Figure 5.13: Temperature fluctuations associated in *pp* and *pPb* collisions.

It is observed that the global temperature fluctuations between the CSPM models and the Tsallis distribution are lower in the cases of higher density and temperature, corresponding to the events in *pp* to 13 TeV and *pPb* to 5.02 TeV.

Chapter 6

Conclusions

In heavy ion collisions, fluctuations commonly have two distinct origins, first, quantum fluctuations which are initial state fluctuations and classical thermodynamical fluctuations. Quantum fluctuatios one are associated to the internal structures of the colliding nuclei, at small time scale, on the contrary initial energy densitites emerge as event-by-event fluctuations in the energy density or temperature.
Thermodynamic fluctuations may have multiple sources, like local thermal fluctuations of energy density, and event-by-event mismatch in the freeze-out conditions other than volume fluctuations, They are then related to several thermodynamic parameters. As an example fluctuation in temperature is related to the heat capacity of the system, based on the temperature of the system at freeze-out.
T_eff has two contributions thermal part (T_kin) and collective transverse velocity ($< \beta T >$) of the system such that $T_eff = T_kin + f(\beta T)$. For pions, one can consider $(\beta T) \approx m_0 < \beta T >^2$. For top central (0–5 %) collisions, the transverse velocity can be assumed to be same for all events due to spherical symmetry for ultra-central collisions, and the fluctuations in the flow velocity can be neglected. Thus the fluctuation in T_eff may be a good representation of the fluctuation in temperature $\delta T_kin = \delta T_eff$ thus connected to the heat capacity.
Usually the multiplicity fluctuations in other observables are treated as a only statistical origin. but here we are talking these emerge multiplicity fluctuations as part of dynamical origin related to the non equilibrium medium formed. In this work we calculate based on data the results for the global temperature associated with the different energies at the LHC that increases with multiplicity in two different approach's in the String Percolation Model modify for small collisions systems, which include size effects and, in the approach, using Tsallis distributions. Results are compared with Heavy Ion results, where one can see that the slope decreases for pPb collisions compare to pp and these effect decreases even more for Pb-Pb collisions.
An increase in the trend is fund for increasing multiplicity for all reported energies. These results shown in figures 5.11 to 5.12 are consistent with the picture that small systems have bigger contribution in fluctuations due to the systems size which is more likely not able to thermalize in such system. Results can further be related to isothermal compressibility as a characterizing quantity of the formed medium.

Bibliography

1. Cleymans, J. & Worku, D. The Tsallis Distribution in Proton-Proton Collisions at $\sqrt{s}$ = 0.9 TeV at the LHC. Publisher: arXiv Version Number: 1. https://arxiv.org/abs/1110.5526 (2023) (2011) (cit. on pp. 3, 5).
2. Lee, T. D. & Wick, G. C. Vacuum stability and vacuum excitation in a spin-0 field theory. *Phys. Rev. D* **9,** 2291–2316. https://link.aps.org/doi/10.1103/PhysRevD.9.2291 (Apr. 1974) (cit. on pp. 7, 17, 18, 23).
3. Lee, T. D. Abnormal nuclear states and vacuum excitation. *Rev. Mod. Phys.* **47,** 267–275. https://link.aps.org/doi/10.1103/RevModPhys.47.267 (Apr. 1975) (cit. on pp. 7, 18).
4. Griffiths, D. J. *Introduction to elementary particles* 2., rev. ed., 5. reprint. 454 pp. ISBN: 978-3-527-40601-2 (Wiley-VCH, Weinheim, 2011) (cit. on p. 9).
5. Chaudhuri, A. *A Short Course on Relativistic Heavy Ion Collisions* ISBN: 978-0-7503-1060-4. http://iopscience.iop.org/book/978-0-750-31060-4 (2020) (IOP Publishing, 2014) (cit. on pp. 9, 14).
6. Brown, L. M. & Rechenberg, H. Nuclear structure and beta decay (1932–1933). *American Journal of Physics* **56,** 982–988. ISSN: 0002-9505, 1943-2909. http://aapt.scitation.org/doi/10.1119/1.15352 (2023) (Nov. 1988) (cit. on p. 9).
7. Giunti, C. & Kim, C. W. *Fundamentals of neutrino physics and astrophysics* OCLC: ocm76935610. 710 pp. ISBN: 978-0-19-850871-7 (Oxford University Press, Oxford ; New York, 2007) (cit. on pp. 10, 11).
8. Weinberg, S. A Model of Leptons. *Physical Review Letters* **19,** 1264–1266. ISSN: 0031-9007. https://link.aps.org/doi/10.1103/PhysRevLett.19.1264 (2023) (Nov. 20, 1967) (cit. on p. 10).
9. Glashow, S. L. Partial-symmetries of weak interactions. *Nuclear Physics* **22,** 579–588. ISSN: 00295582. https://linkinghub.elsevier.com/retrieve/pii/0029558261904692 (2022) (Feb. 1961) (cit. on p. 10).
10. Salam, A. in Ali, A., Isham, C., Kibble, T. & Riazuddin. *World Scientific Series in 20th Century Physics* 244–254 (WORLD SCIENTIFIC, May 1994). http://www.worldscientific.com/doi/abs/10.1142/9789812795915_0034 (2023) (cit. on p. 10).
11. Higgs, P. W. Spontaneous Symmetry Breakdown without Massless Bosons. *Physical Review* **145,** 1156–1163. ISSN: 0031-899X. https://link.aps.org/doi/10.1103/PhysRev.145.1156 (2023) (May 27, 1966) (cit. on p. 10).
12. Higgs, P. Broken symmetries, massless particles and gauge fields. *Physics Letters* **12,** 132–133. ISSN: 00319163. https://linkinghub.elsevier.com/retrieve/pii/0031916364911369 (2023) (Sept. 1964) (cit. on pp. 10, 11).

13. Kibble, T. W. B. Symmetry Breaking in Non-Abelian Gauge Theories. *Physical Review* **155,** 1554–1561. ISSN: 0031-899X. https://link.aps.org/doi/10.1103/PhysRev.155.1554 (2023) (Mar. 25, 1967) (cit. on p. 10).

14. Guralnik, G. S., Hagen, C. R. & Kibble, T. W. B. Global Conservation Laws and Massless Particles. *Physical Review Letters* **13,** 585–587. ISSN: 0031-9007. https://link.aps.org/doi/10.1103/PhysRevLett.13.585 (2023) (Nov. 16, 1964) (cit. on p. 10).

15. Englert, F. & Brout, R. Broken Symmetry and the Mass of Gauge Vector Mesons. *Physical Review Letters* **13,** 321–323. ISSN: 0031-9007. https://link.aps.org/doi/10.1103/PhysRevLett.13.321 (2023) (Aug. 31, 1964) (cit. on p. 10).

16. 't Hooft, G. & Veltman, M. Regularization and renormalization of gauge fields. *Nuclear Physics B* **44,** 189–213. ISSN: 05503213. https://linkinghub.elsevier.com/retrieve/pii/0550321372902799 (2023) (July 1972) (cit. on p. 10).

17. Aad, G. *et al.* Observation of a new particle in the search for the Standard Model Higgs boson with the ATLAS detector at the LHC. *Physics Letters B* **716,** 1–29. ISSN: 03702693. https://linkinghub.elsevier.com/retrieve/pii/S037026931200857X (2023) (Sept. 2012) (cit. on p. 10).

18. Chatrchyan, S. *et al.* Observation of a new boson at a mass of 125 GeV with the CMS experiment at the LHC. *Physics Letters B* **716,** 30–61. ISSN: 03702693. https://linkinghub.elsevier.com/retrieve/pii/S0370269312008581 (2023) (Sept. 2012) (cit. on p. 10).

19. Bettini, A. *Introduction to Elementary Particle Physics* 1st ed. ISBN: 978-0-521-88021-3. https://www.cambridge.org/core/product/identifier/9780511809019/type/book (2023) (Cambridge University Press, May 8, 2008) (cit. on p. 10).

20. CERN. The Standard Model. https://home.cern/science/physics/standard-model (cit. on p. 10).

21. Commons, W. *File:Standard Model of Elementary Particles.svg* 2023. ttps://commons.wikimedia.org/w/index.php?title=File:Standard_Model_of_Elementary_Particles.svg&oldid=746153035 (2023) (cit. on p. 11).

22. Particle Data Group *et al.* Review of Particle Physics. *Progress of Theoretical and Experimental Physics* **2020,** 083C01. ISSN: 2050-3911. https://academic.oup.com/ptep/article/doi/10.1093/ptep/ptaa104/5891211 (2022) (Aug. 14, 2020) (cit. on pp. 11, 12, 16).

23. Dürr, S. *et al.* Ab Initio Determination of Light Hadron Masses. *Science* **322,** 1224–1227. ISSN: 0036-8075, 1095-9203. https://www.science.org/doi/10.1126/science.1163233 (2023) (Nov. 21, 2008) (cit. on p. 11).

24. Bethke, S. Experimental tests of asymptotic freedom. *Progress in Particle and Nuclear Physics* **58,** 351–386. ISSN: 0146-6410. http://www.sciencedirect.com/science/article/pii/S0146641006000615 (2007) (cit. on pp. 11, 14).

25. Greenberg, O. W. Spin and Unitary-Spin Independence in a Paraquark Model of Baryons and Mesons. *Physical Review Letters* **13,** 598–602. ISSN: 0031-9007. https://link.aps.org/doi/10.1103/PhysRevLett.13.598 (2023) (Nov. 16, 1964) (cit. on p. 12).

26. Gell-Mann, M. A schematic model of baryons and mesons. *Physics Letters* **8,** 214–215. ISSN: 00319163. https://linkinghub.elsevier.com/retrieve/pii/S0031916364920013 (2023) (Feb. 1964) (cit. on p. 12).

27. Zweig, G. An SU$_3$ model for strong interaction symmetry and its breaking. Publisher: CERN Document Server. http://cds.cern.ch/record/352337 (2023) (1998) (cit. on p. 12).

28. Ellis, R. K., Stirling, W. J. & Webber, B. R. *QCD and Collider Physics* 1st ed. ISBN: 978-0-521-58189-9. https://www.cambridge.org/core/product/identifier/9780511628788/type/book (2022) (Cambridge University Press, Oct. 24, 1996) (cit. on p. 15).

29. Yndurain, F. J. *Quantum Chromodynamics An Introduction to the Theory of Quarks and Gluons* OCLC: 1196198876. ISBN: 978-3-662-09633-8 (Springer Berlin Heidelberg, S.l., 2013) (cit. on p. 15).

30. Scharenberg, R., Srivastava, B., Hirsch, A. & Pajares, C. Hot Dense Matter: Deconfinement and Clustering of Color Sources in Nuclear Collisions. *Universe* **4,** 96. ISSN: 2218-1997. http://www.mdpi.com/2218-1997/4/9/96 (2023) (Sept. 18, 2018) (cit. on p. 17).

31. Vogt, R. *Ultrarelativistic Heavy-Ion Collisions* OCLC: 1048467929. ISBN: 978-0-08-052536-5 (Elsevier Science, Amsterdam, 2014) (cit. on pp. 17, 18).

32. CERN. *Facts and figures about the LHC* https://home.cern/resources/faqs/facts-and-figures-about-lhc (cit. on p. 17).

33. Busza, W., Rajagopal, K. & Van Der Schee, W. Heavy Ion Collisions: The Big Picture and the Big Questions. *Annual Review of Nuclear and Particle Science* **68,** 339–376. ISSN: 0163-8998, 1545-4134. https://www.annualreviews.org/doi/10.1146/annurev-nucl-101917-020852 (2023) (Oct. 19, 2018) (cit. on pp. 18, 21).

34. Nagle, J. L. & Zajc, W. A. Small System Collectivity in Relativistic Hadronic and Nuclear Collisions. *Annual Review of Nuclear and Particle Science* **68,** 211–235. ISSN: 0163-8998, 1545-4134. https://www.annualreviews.org/doi/10.1146/annurev-nucl-101916-123209 (2023) (Oct. 19, 2018) (cit. on pp. 19, 20).

35. Braun, M. A. *et al.* De-Confinement and Clustering of Color Sources in Nuclear Collisions. Publisher: arXiv Version Number: 1. https://arxiv.org/abs/1501.01524 (2023) (2015) (cit. on pp. 23–25).

36. Isichenko, M. B. Percolation, statistical topography, and transport in random media. *Reviews of Modern Physics* **64,** 961–1043. ISSN: 0034-6861, 1539-0756. https://link.aps.org/doi/10.1103/RevModPhys.64.961 (2023) (Oct. 1, 1992) (cit. on p. 24).

37. Alvarado, J. R., Bautista, I., Fernandez Tellez, A. & Fierro, P. Viscosity of non equilibrium hot & dense QCD drop formed at LHC (cit. on p. 25).

38. Bautista, I., Pajares, C., Milhano, J. G. & de Deus, J. D. Rapidity dependence of particle densities in pp and AA collisions. *Physical Review C* **86,** 034909. ISSN: 0556-2813, 1089-490X. arXiv: 1206.6737[hep-ph,physics:nucl-th]. http://arxiv.org/abs/1206.6737 (2022) (Sept. 24, 2012) (cit. on p. 26).

39. Bautista, I., Milhano, J. G., Pajares, C. & De Deus, J. D. Multiplicity in pp and AA collisions: the same power law from energy–momentum constraints in string production. *Physics Letters B* **715,** 230–233. ISSN: 03702693. https://linkinghub.elsevier.com/retrieve/pii/S0370269312007691 (2023) (Aug. 2012) (cit. on p. 26).

40. Bautista, I., Téllez, A. F. & Ghosh, P. *Indication of change of phase in high-multiplicity proton-proton events at LHC in String Percolation Model* Sept. 8, 2015. arXiv: 1509.02278[hep-ph,physics:nucl-ex,physics:nucl-th]. http://arxiv.org/abs/1509.02278 (2023) (cit. on p. 26).

41. Bazavov, A. *et al.* Chiral and deconfinement aspects of the QCD transition. *Physical Review D* **85,** 054503. ISSN: 1550-7998, 1550-2368. https://link.aps.org/doi/10.1103/PhysRevD.85.054503 (2023) (Mar. 5, 2012) (cit. on p. 27).

42. Tsallis, C. Possible generalization of Boltzmann-Gibbs statistics. *Journal of Statistical Physics* **52,** 479–487. ISSN: 0022-4715, 1572-9613. http://link.springer.com/10.1007/BF01016429 (2023) (July 1988) (cit. on p. 30).

43. Biro, T. S., Purcsel, G. & Urmossy, K. Non-Extensive Approach to Quark Matter. *The European Physical Journal A* **40,** 325. ISSN: 1434-6001, 1434-601X. arXiv: 0812.2104[hep-ph]. http://arxiv.org/abs/0812.2104 (2023) (June 2009) (cit. on p. 30).

44. The CMS Collaboration *et al.* Study of the inclusive production of charged pions, kaons, and protons in pp collisions at $\sqrt{s} = 0.9, 2.76,\mbox{ and }7~\mbox{TeV}$. *The European Physical Journal C* **72,** 2164. ISSN: 1434-6044, 1434-6052. http://link.springer.com/10.1140/epjc/s10052-012-2164-1 (2023) (Oct. 2012) (cit. on pp. 32, 33, 35).

45. Sirunyan, A. M. *et al.* Measurement of charged pion, kaon, and proton production in proton-proton collisions at s = 13 TeV. *Physical Review D* **96,** 112003. ISSN: 2470-0010, 2470-0029. https://link.aps.org/doi/10.1103/PhysRevD.96.112003 (2023) (Dec. 5, 2017) (cit. on pp. 32, 33, 35).

46. The CMS Collaboration *et al.* Study of the production of charged pions, kaons, and protons in pPb collisions at $$\sqrt{s_{NN}} =\; $$ s N N = 5.02 $$\,\text {TeV}$$ TeV. *The European Physical Journal C* **74,** 2847. ISSN: 1434-6044, 1434-6052. http://link.springer.com/10.1140/epjc/s10052-014-2847-x (2022) (June 2014) (cit. on pp. 32–34).

47. Abelev, B. *et al.* Production of charged pions, kaons and protons at large transverse momenta in pp and Pb–Pb collisions at s NN = 2.76 TeV. *Physics Letters B* **736,** 196–207. ISSN: 03702693. https://linkinghub.elsevier.com/retrieve/pii/S0370269314004973 (2022) (Sept. 2014) (cit. on pp. 32–34).

48. Acharya, S. *et al.* Production of charged pions, kaons, and (anti-)protons in Pb-Pb and inelastic p p collisions at s N N = 5.02 TeV. *Physical Review C* **101,** 044907. ISSN: 2469-9985, 2469-9993. https://link.aps.org/doi/10.1103/PhysRevC.101.044907 (2023) (Apr. 29, 2020) (cit. on pp. 32–34).

List of Tables

List of Figures